1   **Gene editing preserves visual function in a mouse model of retinal degeneration**

2   Paola Vagni[1], Laura E. Perlini[2], Naïg A. L. Chenais[1], Tommaso Marchetti[1], Martina Parrini[2], Andrea

3   Contestabile[2], Laura Cancedda[2,3], and Diego Ghezzi[2]

4   [1]Medtronic Chair in Neuroengineering, Center for Neuroprosthetics and Institute of Bioengineering,

5   School of Engineering, École Polytechnique Fédérale de Lausanne, Lausanne, Switzerland.

6   [2]Laboratory of Local Micro-environment and Brain Development, Department of Neuroscience and

7   Brain Technologies, Istituto Italiano di Tecnologia, Genova, Italy.

8   [3]Dulbecco Telethon Institute, Italy

9   Andrea Contestabile, Laura Cancedda, and Diego Ghezzi contributed equally to this work.

10   Correspondence and requests for materials should be addressed to D.G. (email: diego.ghezzi@epfl.ch).

11

12   **Abstract**

13   Inherited retinal dystrophies are a large and heterogeneous group of degenerative diseases caused by

14   mutations in various genes. Given the favourable anatomical and immunological characteristics of the

15   eye, gene therapy holds great potential for their treatment. We used a tailored CRISPR/Cas9-based gene

16   editing system to prevent retinal photoreceptor death in the Rd10 mouse model of retinitis pigmentosa.

17   We tested the gene editing tool *in vitro* and then used *in vivo* subretinal electroporation to deliver it to

18   one of the retinas of mouse pups at different stages of photoreceptor differentiation. Three months after

19   gene editing, the treated eye exhibited a higher visual acuity compared to the untreated eye. Moreover,

20   we observed preservation of light-evoked responses both in explanted retinas and in the visual cortex

21   of treated animals. Our study validates a CRISPR/Cas9-based therapy as a valuable new approach for

22   the treatment of retinitis pigmentosa caused by autosomal recessive loss-of-function point mutations.

23 **Introduction**

24 Retinitis pigmentosa is a group of inherited retinal dystrophies (IRDs) that cause the progressive death

25 of retinal photoreceptors and eventually blindness(Ferrari et al., 2011). The treatment of retinitis

26 pigmentosa is still a major challenge because of the early death of rod photoreceptors and the late onset

27 of the symptoms. Daily vision in humans mainly depends on cone photoreceptors, which in retinitis

28 pigmentosa degenerate only at a late stage: likely because cones metabolically depend on rods, which

29 provide them nutrients(Narayan et al., 2016). Therefore, acting on the principal cause of degeneration,

30 namely at the level of rod photoreceptors, would be an effective therapeutic approach to preserve vision

31 in retinitis pigmentosa. Notably, rod-rich photoreceptor transplantations can halt cone loss in

32 degenerating retinas(Mohand-Said et al., 2000).

33 Mutations in the β-domain of the phosphodiesterase 6 (*PDE6B*) gene, which hydrolyses cyclic

34 guanosine monophosphate (cGMP) and initiates phototransduction, are among the most commonly

35 identified causes of autosomal recessive retinitis pigmentosa(DANCIGER et al., 1995; McLaughlin et

36 al., 1995). Missense mutations in *PDE6B* lead to photoreceptor death, triggered by the toxic

37 accumulation of cGMP(Ulshafer et al., 1980), and result in a progressive loss of visual function, starting

38 from the peripheral retina and progressing towards the centre. The discovery of naturally occurring

39 mouse models carrying mutations on the *Pde6b* gene(Chang et al., 2002; 2007) has provided a better

40 understanding of the mechanisms underlying retinal degeneration and has prompted the development

41 of new therapies. The retinal degeneration 10 (Rd10) mouse carries an autosomal recessive loss-of-

42 function missense point mutation in the *Pde6b* gene (exon 13; C1678T → R560C), leading to the

43 progressive degeneration of photoreceptor cells. Rd10 mice are particularly useful as an animal model

44 for autosomal recessive retinitis pigmentosa since the slow degeneration of photoreceptor cells

45 recapitulates the time course of the disease in patients.

46 The first genetic approaches to vision restoration in the Rd10 mouse was based on virus-mediated

47 supplementation of the *Pde6b* gene(Bennett et al., 1996; Jomary et al., 1997; Pang et al., 2008; 2012).

48 Similarly, viral gene transfer therapies have led to promising results for Leber Congenital Amaurosis 2

49 and some other retinal diseases, as demonstrated by the several ongoing clinical trials(Auricchio et al.,

2

50 2017). Recently, gene editing tools based on Clustered Regularly Interspaced Short Palindromic

51 Repeats (CRISPRs)-Associated (Cas) Genes have completely revolutionised gene therapy(Heidenreich

52 and Zhang, 2016). The Cas9 nuclease utilises a guide RNA (gRNA) to induce DNA Double-Strand

53 Breaks (DSBs) at a precise location in the target genomic site. CRISPR/Cas9 system is easily tuneable,

54 versatile, and enables the precise correction of genetic defects directly on the patient genome. The

55 CRISPR/Cas9 system can either be used to disrupt the target gene by Non-Homologous End-Joining

56 (NHEJ) of DSBs or to edit the target gene by Homology Directed Repair (HDR) in the presence of a

57 DNA donor sequence (repair template). Importantly, the expression of the CRISPR/Cas9 system is only

58 needed for the relatively short period necessary to correct the genetic mutation (a few days, rather than

59 continuously as in the case of gene supplementation therapies)(Ran et al., 2013).

60 In this study, we designed a CRISPR/Cas9 gene editing system that can repair the genetic mutation in

61 the Rd10 mouse model taking advantage of the increased activity of the HDR mechanism in dividing

62 progenitor cells(Saleh-Gohari and Helleday, 2004). We tested the efficiency of the designed approach

63 first *in vitro* and then *in vivo*. To demonstrate the phenotype reversal, we performed behavioural and

64 electrophysiological analysis on treated and control mice. Overall, the treated mice retained 50 % of the

65 normal visual acuity even three months after the treatment.

66 **Results**

67 ***gRNA screening and high editing efficiency of the CRISPR-Cas9 vector in cell culture.*** The

68 efficiency of different gRNAs in inducing HDR-mediated editing of a specific genomic locus can be

69 very different, ranging from 0.7 to 30 %(Cong et al., 2013; Ran et al., 2013). Therefore, as a first step

70 in the development of the gene editing system, we designed and screened different gRNAs for their

71 ability to induce CRISPR/Cas9-mediated editing of the *Pde6b* gene. We selected three candidate

72 gRNAs and screened them in mouse Neuro 2A (N2A) cells to determine which one was the best at

73 targeting the sequence coding for WT *Pde6b*. We transfected N2A cells with a single plasmid,

74 containing Cas9, one of the three gRNAs, and the green fluorescent protein (GFP), along with a DNA

75 single-stranded oligonucleotide (ssODN) repair template specific for each gRNA, containing flanking

76 sequences of 100 bp on each side of the insertion site that were homologous to the target region. The

3

77   gRNA #1 and gRNA #3 mapped upstream and downstream to the Rd10 locus, while the gRNA #2

78   mapped directly on it (**Fig. 1a**). Each repair template for HDR-mediated editing was designed to edit

79   the genomic DNA (gDNA) sequence at the Rd10 locus and simultaneously remove an adjacent cutting

80   site for the restriction enzyme BanI (by introducing a silent mutation), allowing the assessment of the

81   editing efficiency by BanI restriction analysis (**Fig 1a**). Moreover, each repair template also carried a

82   second specific silent mutation in the PAM sequence of the corresponding gRNA to avoid further Cas9-

83   mediated cutting on the edited genomic sequence (**Fig. 1a**). One day after transfection, we isolated

84   GFP-expressing cells by fluorescent activated cell sorting (FACS), extracted the gDNA and PCR-

85   amplified a 700 bp fragment containing the *Pde6b* target region with primers mapping outside the

86   ssODN homology arm sequence (**Fig. 1a**). After BanI digestion and agarose-gel electrophoresis, the

87   edited DNA appeared as a single uncut band (700 bp), while non-edited DNA was digested in two

88   fragments (230 and 470 bp). The quantification of the percentage of edited versus non-edited DNA for

89   each gRNA showed that gRNA #2 had the highest editing efficiency and was the best performing gRNA

90   (**Fig. 1b,c**). Based on this result, we next designed for the final editing tool gRNA #4 which differ from

91   gRNA #2 only in a single base pair (**Fig. 1d**), corresponding to the C to T mutation found in the mutated

92   *Pde6b* gene of Rd10 mice. We further verified gRNA #4 editing efficiency in neural stem cells (NSC)

93   derived from Rd10 homozygous pups. The transfected Rd10 cells were selected for GFP-expression

94   with FACS and the editing efficiency was evaluated by BanI restriction assay, as described above for

95   N2A cells. We found a mean (± s.d., $n = 3$) net editing efficiency of 39.3 ± 6.4 % in NSC harbouring

96   the Rd10 mutation (**Fig. 1e,f**). These data indicate that the selected gRNA #4 efficiently targets the

97   Rd10 mutation in the *Pde6b* gene and that the correct sequence can be restored with high efficiency by
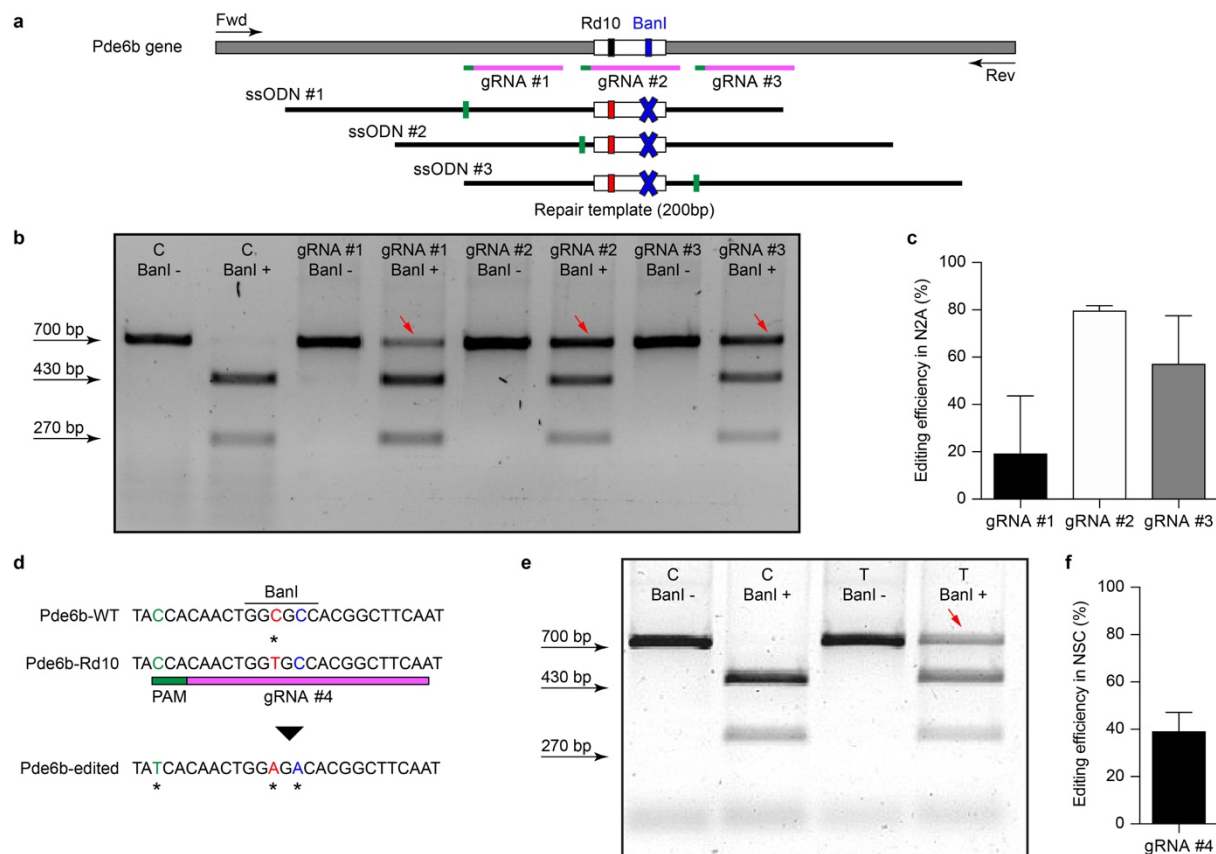
98   CRISPR/Cas9-mediated HDR editing.

4

99

Figure 1. Screening of gRNAs targeting the Rd10 locus. a, Schematic representation (not in scale) of the mouse *Pde6b* gene showing the position of the three gRNAs tested (in magenta with green PAM sequence), the ssODN repair templates (black), and the PCR primers used for screening (arrows). The white rectangle represents the target editing region with Rd10 mutation (black/red) and the BanI cutting site (blue). Each ssODN also carries a silent mutation in the corresponding gRNA PAM sequence (green). **b,** Representative example of an agarose gel electrophoresis of the BanI restriction assay from transfected (T) and control (C) mouse N2A cells. Unedited DNA is cut in two fragments by BanI digestion (470 and 230 bp), while edited DNA is not cut by the restriction enzyme (700 bp band, red arrows). **c**, Quantification of the mean (± s.d., *n* = 2) editing efficiency for the three gRNA in N2A cells. **d,** Schematic representation of editing strategy for gRNA #4 targeting the Rd10 mutation. The HDR strategy was designed to edit the DNA sequence (in red), while introducing a silent mutation in the cutting sequence for BanI (in blue). A second silent mutation in the PAM sequence of the gRNA (in green) is included in the repair template in order to avoid further Cas9-mediated cutting on the edited genomic sequence. **e,** Representative example of an agarose gel electrophoresis of the BanI restriction assay for gRNA #4 transfected (T) and control (C) NSC from Rd10 mice. The red arrow indicates the edited DNA that is resistant to BanI digestion. **c**, Quantification of the mean (± s.d., *n* = 3) editing efficiency for gRNA #4 in Rd10 NSC.

5

117 ***Efficient delivery of a reporter gene to photoreceptor cells by in vivo electroporation.*** The efficiency

118 of electrotransfer depends on various factors such as the cell size, the parameters of the electric pulses,

119 and the phase of the cell cycle. The latter has to be taken into account especially when interested in

120 targeting the highest number of cells and in exploiting the HDR mechanism to achieve gene editing. In

121 order to obtain the highest number of transfected cells without inducing eye defects, we performed pilot

122 experiments to optimise the electroporation protocol and select the best timing for delivery. Although

123 electroporation immediately after birth is potentially more efficient, it can result in eye damage: in our

124 hand, postnatal day (P) 1 electroporation resulted in more than 50 % of the pups bearing eye defects as

125 adults, while this percentage was reduced at 40 % by performing electroporation at P3 (at the peak of

126 the photoreceptor proliferation curve). For this reason, P3 was selected for the *in vivo* experiments (**Fig.**

127 **2a,** dashed line). Moreover, several groups reported efficient retinal electroporation in neonatal mice

128 using five pulses of 50 ms at 80 V (1 Hz)(Matsuda and Cepko, 2004; de Melo and Blackshaw, 2011),

129 but we found this protocol to cause eye defects (possibly affecting visual functions) in 40 % of the adult

130 mice when the electroporation was performed at P3. Thus, based on previous observations in cell

131 cultures(Bureau et al., 2000), we tested a different protocol (**Fig. 2b**) consisting of two short poring

132 pulses at high voltage (5 ms, 100 V, 0.1 Hz) followed by five long transfer pulses at a lower voltage

133 (50 ms, 30 V, 1 Hz). Applying this improved protocol, we obtained an electroporation efficiency

134 comparable to the standard protocol, whereas the number of pups bearing eye defects when adults

135 decreased from 40 to 5 %; those animals were excluded from the experiments. Also, the use of a

136 conductive gel between the electrode plate and the tissue increased the conductivity and avoided

137 burning marks on the cornea. In order to assess the efficiency of electroporation in targeting the

138 photoreceptor cell progenitors *in vivo*, we delivered a plasmid coding for eGFP to the subretinal space

139 of Rd10 mouse pups with two consecutive subretinal injections followed by electroporation at P3 (**Fig.**

140 **2c**). The image sequence shows that eGFP was expressed at all the different stages of retinal

141 development at which the retinas were isolated: P5, P10, and P15 (n = 6 at each time point). At P5, most

142 of the expressing cells were confined to the ventricular zone (VZ), where the photoreceptor progenitors

143 proliferate. At P10, the cells started to migrate towards the photoreceptor layer, which they finally

144 reached by P15. The electroporation targets mostly photoreceptors due to their proximity to the injection

6

145   site, but it is not completely specific to this cell type; indeed, we observed some bipolar and ganglion

146   cells expressing eGFP. This eventuality does not represent a concern for the outcome of the therapy

147   since the targeted gene is expressed specifically in rod photoreceptors. To analyse the extension of the

148   electroporated zone, we prepared wholemount retinas from the treated mice (**Fig. 2d**). In a few cases (2

149   out of 6) the two consecutive injections per eye resulted in two electroporated areas and all the other

150   cases in one area only, with a single area covering up to 25 % of the retina. The localisation of the

151   electroporated cells depends on the orientation of the electric field to the injection site at the moment of

152   the electroporation, which is challenging to control in an animal as small as the mouse, especially at

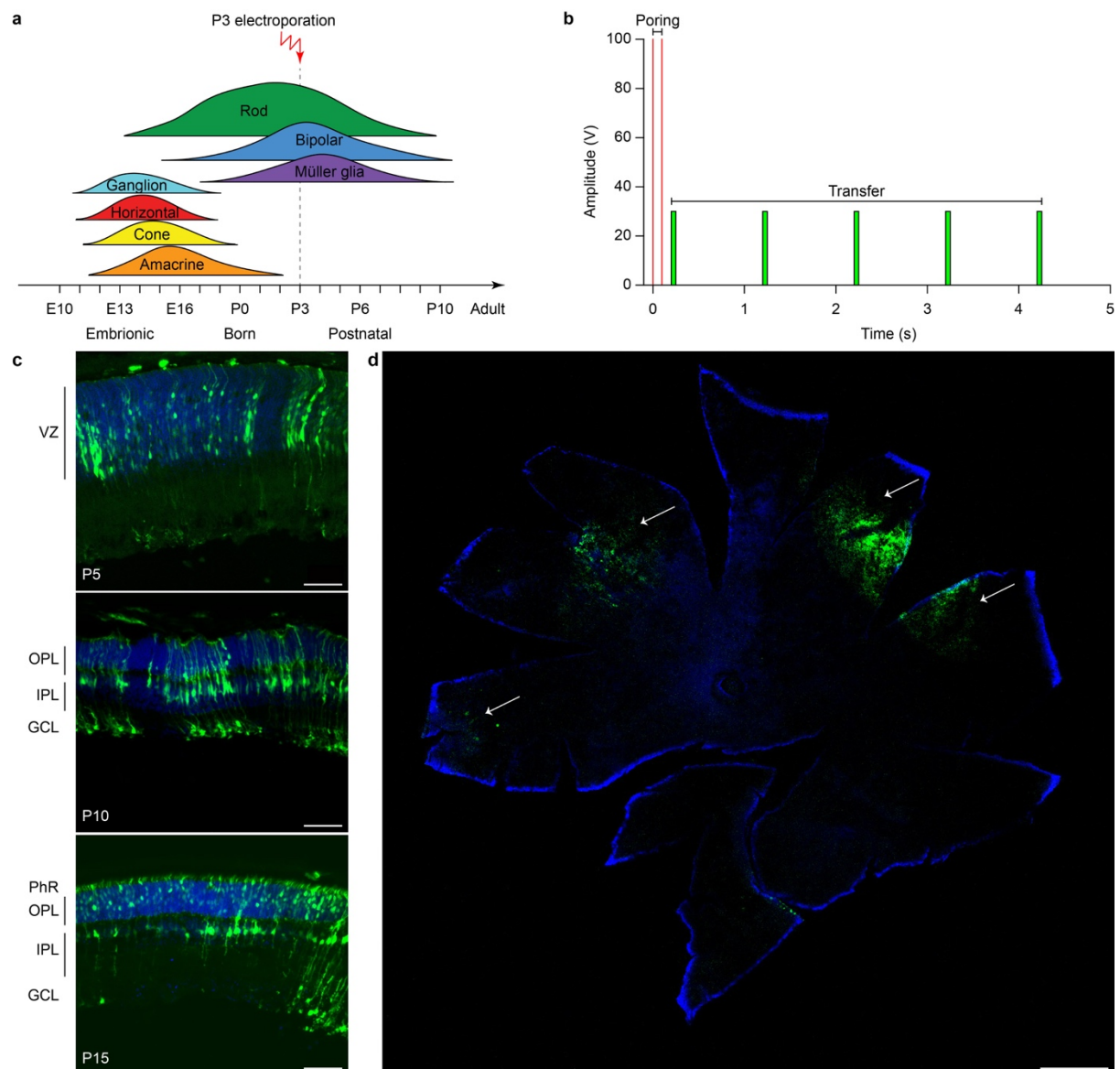153   this young age.

154

7

155 **Figure 2. Electroporation of photoreceptor progenitor cells *in vivo* at P3. a,** The graph shows the
156 proliferation period for all the retinal cell types Sketch redrawn from(Zhang et al., 2011). The
157 proliferation of rod photoreceptors has a peak at birth (P0-P3) and continues until P10. The
158 electroporation was performed at P3. **b,** Schematic representation of the protocol used for
159 electroporation. Two high voltage poring pulses (5 ms, 100 V, 0.1 Hz) are followed by five low voltage
160 transfer pulses (50 ms, 30 V, 1 Hz). **c,** Retinal sections from Rd10 mice electroporated at P3 and
161 collected at different time points, starting from the top: P5, P10, and P15. The scale bar is 60 µm. On
162 the side, the ventricular zone (VZ), the photoreceptor layer (PhR), the outer plexiform layer (OPL), the
163 inner plexiform layer (IPL), and the ganglion cell layer (GCL) are reported. **d,** Representative
164 wholemount retina electroporated at P3 and collected at P10 illustrating the spread of the electroporation
165 (white arrows). The scale bar is 500 µm.

166 ***Significant editing efficiency in vivo of the CRISPR-Cas9 editing tool.*** Evaluating editing efficiency
167 in whole retinas *in vivo* is a more challenging task than *in vitro* due to the presence of a mixed population
168 of transfected and non-transfected cells. To this aim*,* we developed a sensitive droplet digital PCR
169 (ddPCR) assay with two fluorescent probes specific for the edited and unedited alleles (**Fig. 3a**). Rd10
170 pups were electroporated at P3 with plasmids encoding eGFP, Cas9, gRNA #4, together with the ssODN
171 repair template. Sham electroporation of control retinas in Rd10 pups at P3 was performed by omitting
172 the gRNA. Three days after electroporation, we extracted the gDNA from whole retinas and analysed
173 the editing efficiency at the *Pde6b* gene by ddPCR. We found that the mean ($\pm$ s.d., $n = 10$) *in vivo*
174 editing efficiency in Rd10 treated retinas was 0.22 ± 0.14 % and significantly different from Rd10 sham
175 retinas ($p < 0.05$, unpaired t-test) that however showed a low but detectable background (0.057 ± 0.050
176 %, $n = 6$) in the assay (**Fig. 3b**). Although *in vivo* editing efficiency appeared much lower than *in vitro*,
177 this represents an underestimation because the assay was conducted on gDNA extracted from whole
178 retinas that contained only a relatively small percentage of transfected cells. Moreover, treated retinas
179 showed variable degrease of editing, likely due to a difference in electroporation efficiency. However,
180 even a few functional photoreceptors can make a large difference when it comes to visual
181 performance(MacLaren et al., 2006; Tucker et al., 2011).
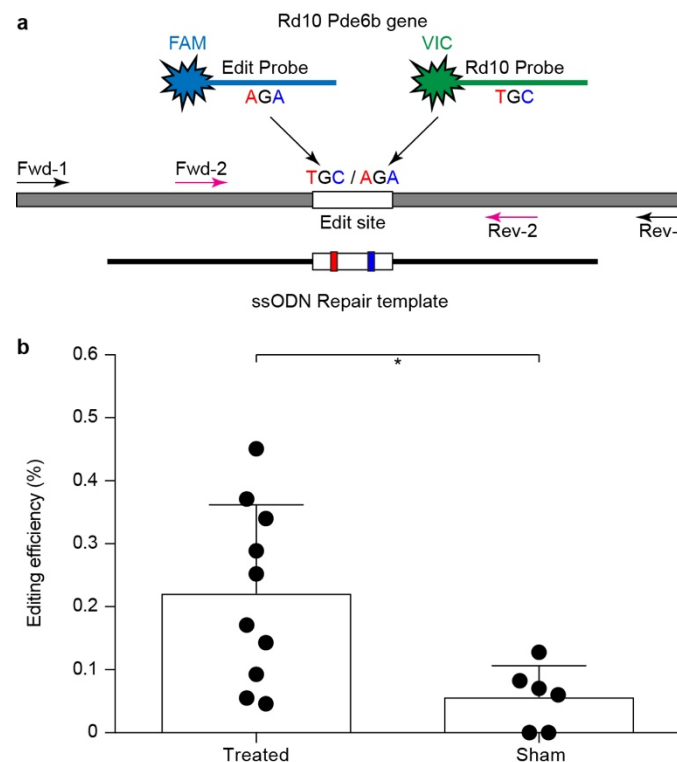
8

Figure 3. Editing efficiency in vivo. **a**, Schematic representation of the ddPCR assay used to quantify *in vivo* editing efficiency. The *Pde6b* gene is in grey and the ssODN repair template in black (not in scale). The white rectangle represents the target editing region. Black and magenta arrows indicate primers pairs used for the nested-ddPCR. Red and blue letters indicate base mismatches detected by the two specific fluorescent probes for the edited and unedited alleles (blue and green respectively). **b**, Quantification of the mean (± s.d.) percentage of editing in Rd10 treated retinas.

Gene editing preserves microelectroretinograms ex vivo at P60. To verify whether the extent of gene editing can translate to improved retinal functionality, we recorded the microelectroretinograms (µERGs) from explanted retinas of P60 Rd10 mice that were electroporated at P3 (**Fig. 4a**). Untreated Rd10 mice were used as control. Previous results show that Rd10 retinas are completely degenerated(Jae et al., 2013) and stop consistently responding to light stimulation at P60(Stasheff et al., 2011). We recorded simultaneously from all the electrodes of a multielectrode array (MEA) while stimulating using green light pulses (4 ms, 0.5 mW mm^{-2}). In **Fig. 4b,** we present a representative µERG response from a treated retina, as the average over ten sequential stimulations delivered at 1 Hz of repetition rate. The a-wave peak amplitudes in Rd10 treated retinas are significantly higher ($p < 0.0001$, unpaired t-test) than Rd10 untreated retinas (**Fig. 4c**). This result supports our hypothesis that the functionality of the retina is preserved in Rd10 treated mice.
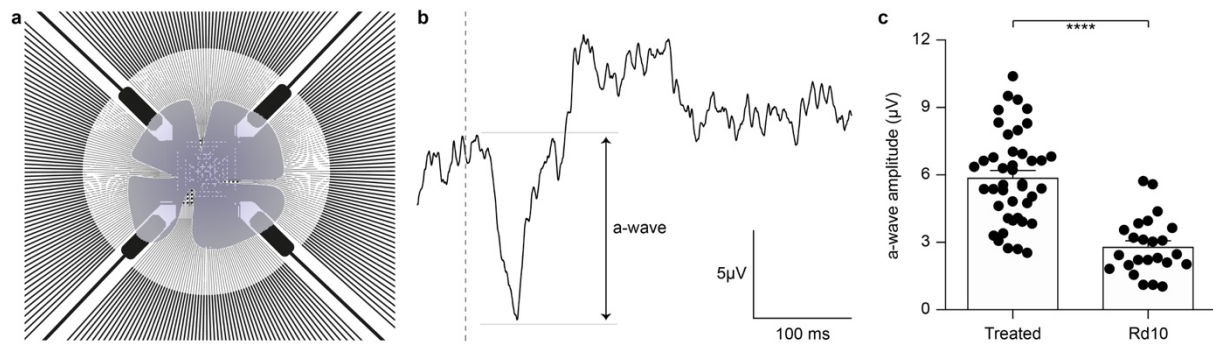
9

Figure 4. Preservation of microelectroretinograms at P60. a, Schematic representation of the experiment. The retina was dissected and placed on a transparent MEA with the retinal ganglion cell side down in contact with the electrodes. The retina was stimulated using green light pulses coming from the bottom. **b,** Representative recording from a Rd10 retina treated at P3. **c,** Quantification of the mean (± s.e.m.) amplitude of the a-wave in the two experimental groups: Rd10 treated (5.89 ± 0.31, n = 42 channels from 2 retinas) and Rd10 untreated (2.81 ± 0.26, n = 27 channels from 2 retinas) retinas.

Gene editing preserves visual acuity in vivo until P90. Next, we verified whether our results *ex vivo* could effectively lead to functional improvement of vision *in vivo*. To this end, we assessed the visual acuity of Rd10 unilaterally treated (at P3), Rd10 unilaterally sham-treated (at P3), Rd10 untreated, and WT adult mice using a behavioural assay. The optomotor test, which measures the integrity of the subcortical visual pathways, uses the amplitude of the optomotor reflex to evaluate the visual acuity of rodents (**Fig. 5a**). In particular, it allows the distinction between right eye-driven and left eye-driven responses, measuring the visual threshold of each eye independently(DOUGLAS et al., 2005). At P30 (about 1 month after treatment), in Rd10 mice, the treated eye (**Fig. 5b**, white circles) showed a higher visual acuity compared to the paired untreated eye (treated 0.24 ± 0.01 C/°, untreated 0.14 ± 0.01 C/°; n = 71, p < 0.0001, Mann-Whitney test). Conversely, the Rd10 sham-treated eye (light grey circles) did not show any improvement compared to the paired untreated eye (sham 0.11 ± 0.01 C/°, untreated 0.13 ± 0.01 C/°; n = 20, p = 0.2306, unpaired t-test). In both WT (left 0.41 ± 0.01 C/°, right 0.39 ± 0.01 C/°; n = 32, p = 0.1009, Mann-Whitney test; black dots) and Rd10 (left 0.12 ± 0.01 C/°, right 0.11 ± 0.01 C/°; n = 47, p = 0.4908, unpaired t-test; dark grey dots) mice no difference was detected between the left and right eyes (**Fig. 5b**). Measures of the optomotor reflex (**Fig. 5c**) demonstrated that the average visual acuity in the treated eyes of Rd10 mice is significantly higher than the average visual acuity of both Rd10 mice (p < 0.0001; One Way ANOVA, Tukey's multiple comparisons test) and sham-treated

10

224 eyes in Rd10 mice (p < 0.0001; One Way ANOVA, Tukey's multiple comparisons test). Sham-treated

225 eyes have a visual acuity not statistically different from Rd10 mice's eyes (p = 0.9849; One Way

226 ANOVA, Tukey's multiple comparisons test). Since it was not measured in dark-adapted conditions,

227 the outcome of the optomotor test is essentially related to the integrity of cone cells and direction-

228 selective retinal ganglion cells. However, the visual acuity measured with this test is reportedly

229 decreasing in Rd10 mice, already starting from P30(Prusky et al., 2004), which matches our data from

230 control and sham mice. We can thus attribute any further preservation of visual acuity to a protective

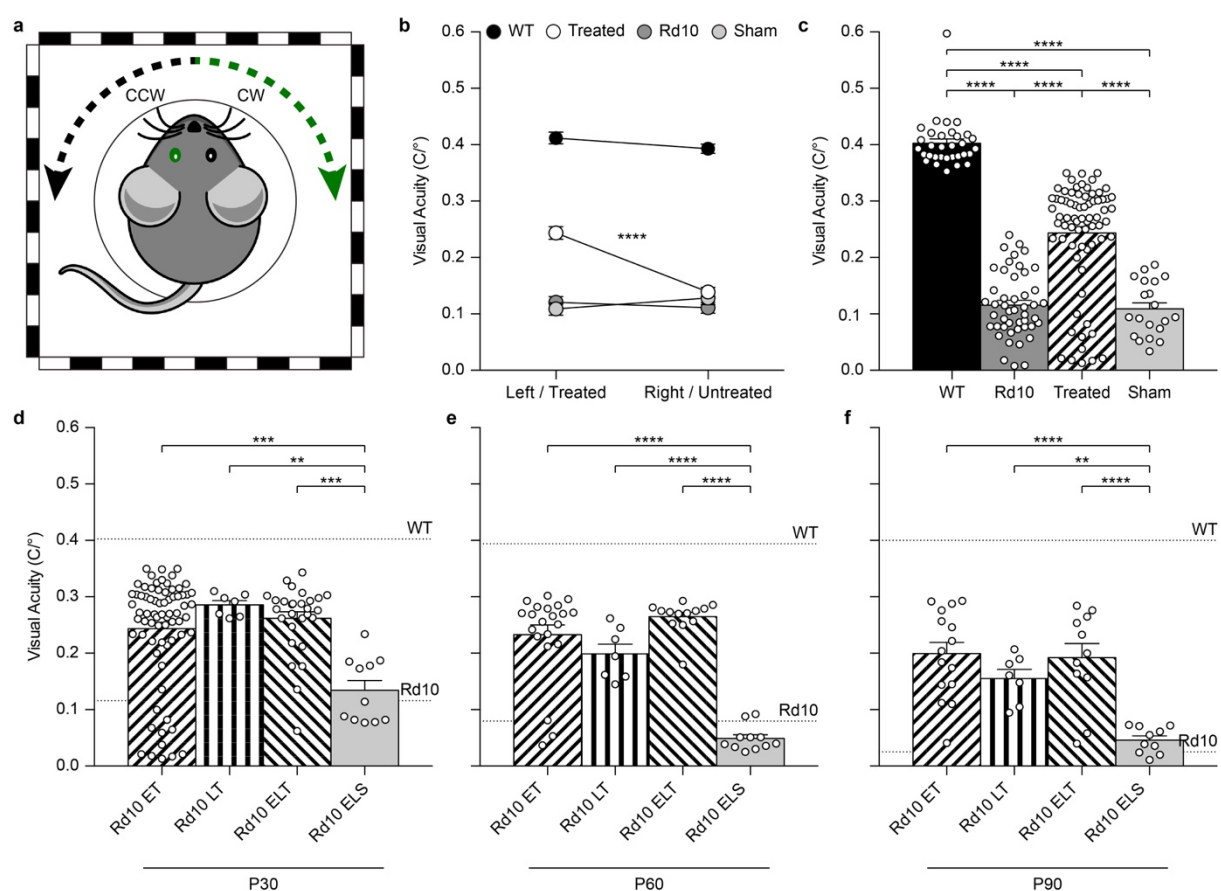231 effect of the treatment.

232

233 **Figure 5. Preservation of the visual acuity in Rd10 treated mice. a,** For each mouse, both the clock-

234 wise (CW, left eye) and counter clock-wise (CCW, right eye) responses were assessed. The sketch

235 represents a mouse with treatment (green) in the left eye (corresponding to the CW response). **b,** Mean

236 (± s.e.m.) visual acuity in WT mice (black circles), untreated Rd10 mice (dark grey circles), Rd10

237 treated mice (white circles), and Rd10 sham-treated mice (light grey circles). **c,** Statistical comparison

238 among the 4 groups (p < 0.0001, One Way ANOVA): WT (0.40 ± 0.01 C/°, n = 32, averaged left and

239 right responses), Rd10 (0.12 ± 0.01 C/°, n = 47, averaged left and right responses), Rd10 treated (0.24

240 ± 0.01 C/°, $n = 71$), and Rd10 sham (0.11 ± 0.01 C/°, $n = 20$). **d**, Statistical comparison (p < 0.001, One

241 Way ANOVA) of the mean (± s.e.m.) visual acuity among Rd10 ET (0.24 ± 0.01 C/°, $n = 71$), Rd10

242 LT (0.29 ± 0.01 C/°, $n = 7$), Rd10 ELT (0.26 ± 0.01 C/°, $n = 28$), and Rd10 ELS (0.13 ± 0.02 C/°, n =

243 11) at P30. **e**, Statistical comparison (p < 0.0001, One Way ANOVA) of the mean (± s.e.m.) visual

244 acuity among Rd10 ET (0.23 ± 0.02 C/°, $n = 21$), Rd10 LT (0.20 ± 0.02 C/°, $n = 7$), Rd10 ELT (0.26 ±

245 0.01 C/°, $n = 13$), and Rd10 ELS (0.05 ± 0.02 C/°, $n = 11$) at P60. **f**, Statistical comparison (p < 0.0001,

246 One Way ANOVA) of the mean (± s.e.m.) visual acuity among Rd10 ET (0.20 ± 0.02 C/°, $n = 15$),

247 Rd10 LT (0.15 ± 0.02 C/°, $n = 7$), Rd10 ELT (0.20 ± 0.03 C/°, $n = 11$), and Rd10 ELS (0.05 ± 0.02 C/°,

248 $n = 10$) at P90. In panels **c-f**, each circle represents a single mouse.

249 We next investigated whether the same treatment could be effective at a later stage of photoreceptor

250 differentiation. To this end, we treated mice at P8 (**Supplementary Fig. 1a**), approximately at the end

251 of the progenitor cells proliferation curve(Zhang et al., 2011). Electroporation at P8 did not result in

252 any eye damage. After the electroporation at P8, the eGFP fluorescence could be detected in retinas of

253 P10 and P15 mice (**Supplementary Fig. 1b,c**).
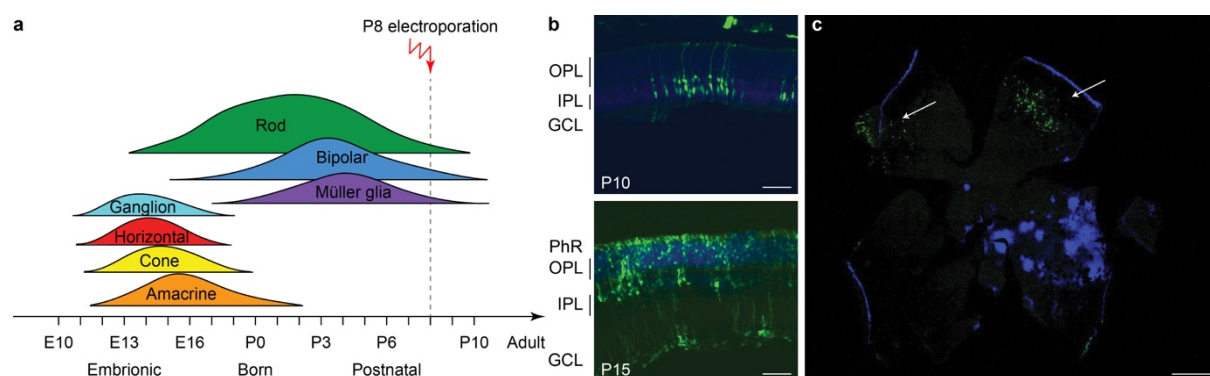
255 **Supplementary Figure 1. Electroporation *in vivo* of photoreceptor progenitor cells at P8. a,** Sketch

256 of the late electroporation time point (P8), at the end of the proliferation period. **b,** Retinal sections from

257 mice electroporated at P8. The sections were collected at two time points after electroporation: P10 and

258 P15. The scale bar is 60 μm. On the side, the photoreceptor layer (PhR), the outer plexiform layer

259 (OPL), the inner plexiform layer (IPL), and the ganglion cell layer (GCL) are reported. **c,** Wholemount

260 retina electroporated at P8 and collected at P15, illustrating the spread of the electroporation (white

261 arrows). The scale bar is 500 μm.

262 Based on this result, we assessed the impact of the period of treatment on the optomotor reflex. We

263 compared the optomotor reflex responses of Rd10 mice upon electroporation at P3 (Rd10 Early Treated,

264 ET), P8 (Rd10 Late Treated, LT), or P3 and P8 (Rd10 Early/Late Treated, ELT). The first treatment

265 corresponds to the peak of the rod's proliferation curve, the second one to the end of the curve, and the

12

266   last treatment to the combination of the two (**Fig. 5d**). As for the Rd10 ET mice (**Fig. 5b**), also for the

267   Rd10 LT (**Supplementary Fig. 2a**) and the Rd10 ELT (**Supplementary Fig. 2b**), the visual acuity

268   measured in the treated eyes was significantly higher than the visual acuity of the paired untreated eyes.

269   Conversely, in Rd10 Early/Late Sham (Rd10 ELS) treated mice the visual acuity was not different

270   between injected and not injected eyes (**Supplementary Fig. 2c**).

271
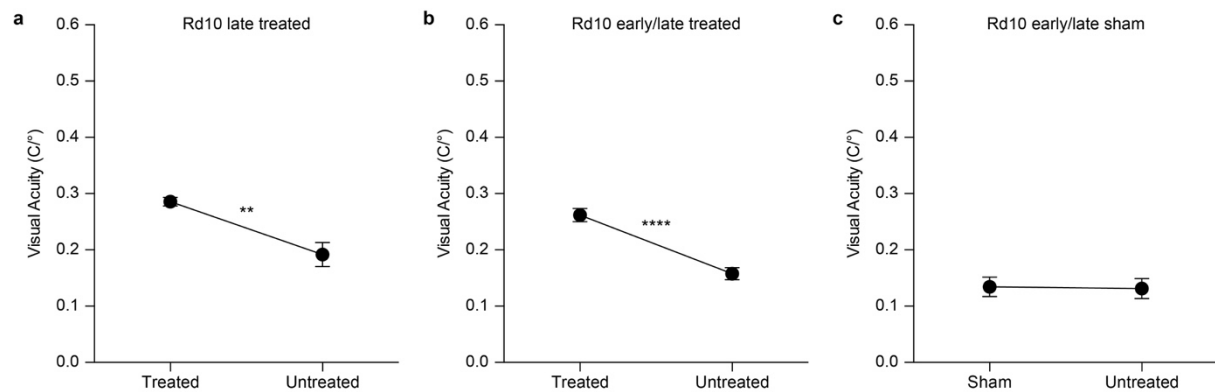
Supplementary Figure 2. Optomotor reflex upon electroporation at P8. a, Mean ($\pm$ s.e.m.) visual acuity in Rd10 mice treated at P8 (Rd10 LT; treated eye 0.29 ± 0.01 C/°, untreated eye 0.19 ± 0.02 C/°; $n = 7$, $p < 0.01$, unpaired t-test). **b**, Mean ($\pm$ s.e.m.) visual acuity in Rd10 mice treated at P3 and P8 (Rd10 ELT; treated eye 0.26 ± 0.01 C/°, untreated eye 0.16 ± 0.01 C/°; $n = 28$, $p < 0.0001$, unpaired t-test). **c**, Mean ($\pm$ s.e.m.) visual acuity in Rd10 mice sham treated at P3 and P8 (Rd10 ELS; sham eye 0.13 ± 0.02 C/°, untreated eye 0.13 ± 0.02 C/°; $n = 11$, $p = 0.8992$, unpaired t-test).

278   Last, we verified the long-term preservation of visual acuity by repeating the optomotor test at P60 and

279   P90. Interestingly, while the visual acuity dropped drastically in untreated and sham-treated Rd10 mice

280   at P60, it did not show a significant decline in any of the treated groups (**Fig. 5e**). At P90, the visual

281   acuity eventually decreased also in treated mice, but overall all the treated groups retained about 50 %

282   of their initial value (**Fig. 5f**). This result shows a preserved functionality of subcortical visual pathways

283   up to 3 months in treated mice at both P3 and P8.

284   ***Gene editing preserves flash-evoked cortical responses at P90.*** To assess the functionality of the

285   retino-cortical visual pathway, we recorded visually-evoked cortical potentials (VEPs) from both

286   hemispheres upon flash stimulation. In **Fig. 6a,** we show a representative trace for each experimental

287   group. For treated and sham-treated Rd10 mice, the representative recordings are relative to the cortex

288   contralateral to the injected eye, since in the mouse the majority of the projections decussate at the optic

13

289   chiasm(Coleman et al., 2009). Since we cannot exclude completely the input coming from the untreated

290   eye (ipsilateral projection), we compared the results of the treated mice with the ones from Rd10 and

291   sham-treated animals to isolate the contribution of the therapy. The mean prominence of the response's

292   peaks was computed. At P90, Rd10 animals show a complete retinal degeneration with very few spared

293   photoreceptors(Gargini et al., 2007; Pennesi et al., 2012). Accordingly, we observed an almost flat

294   response in untreated (Rd10) and sham-treated (Rd10 ES and Rd10 ELS) mice. Conversely, when

295   recording from all the treated groups (Rd10 ET, Rd10 LT, and Rd10 ELT), we observed preservation

296   of the peak prominence in the visual response of the contralateral cortex (**Fig. 6b**). This is indicative of

297   a preserved functionality of cortical visual pathways ($p < 0.0001$; Kruskal-Wallis, Dunns multiple

298   comparison test). In the ipsilateral cortex (**Fig. 6c**), the only significant difference was between WT and

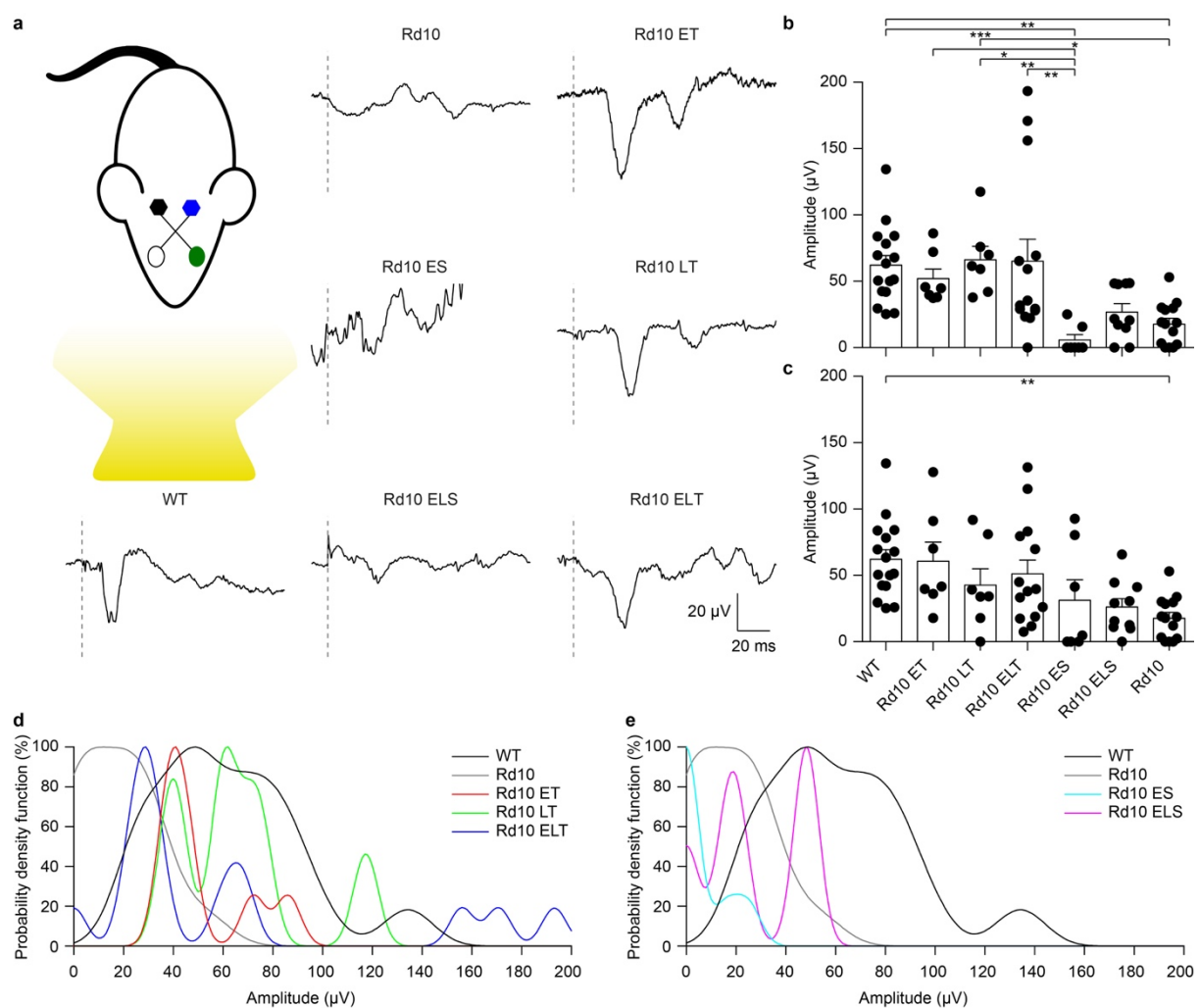299   Rd10 ($p < 0.01$; Kruskal-Wallis, Dunns multiple comparison test).


300

301 **Figure 6. Preservation of visually evoked potentials at P90. a,** Sketch of the recording setup in which
302 the cortex contralateral to the treated eye (green) is in black, while the ipsilateral is in blue.
303 Representative VEP response for each experimental group. The grey dashed lines are the occurrence of
304 the flash. For treated (Rd10 ET, Rd10 LT, and Rd10 ELT) and sham-treated (Rd10 ES and Rd10 ELS)
305 mice, the traces are from the contralateral cortex, while for WT and Rd10 mice the responses of the two
306 cortices were averaged. **b,** Mean ($\pm$ s.e.m.) contralateral peak amplitude for all the experimental groups:
307 WT (91.7 ± 11.1 µV, $n = 16$), Rd10 ET (62.4 ± 9.4 µV, $n = 7$), Rd10 LT (73.1 ± 10.8 µV, $n = 7$), Rd10
308 ELT (71.7 ± 15.2 µV, $n = 14$), Rd10 ES (13.7 ± 8.9 µV, $n = 7$), Rd10 ELS (34.4 ± 7.1 µV, $n = 10$), and
309 Rd10 (23.8 ± 5.5 µV, $n = 14$). **c,** Mean ($\pm$ s.e.m.) ipsilateral peak amplitude for all the experimental
310 groups: WT (91.7 ± 11.1 µV, $n = 16$), Rd10 ET (69.6 ± 14.4 µV, $n = 7$), Rd10 LT (49.8 ± 12.8 µV, $n = $
311 7), Rd10 ELT (96.6 ± 20.7 µV, $n = 14$), Rd10 ES (48.0 ± 21.9 µV, $n = 7$), Rd10 ELS (30.8 ± 7.0 µV, n
312 $= 10$), and Rd10 (23.8 ± 5.5 µV, $n = 14$). In **b** and **c,** for WT and Rd10 mice the responses of the two
313 cortices were averaged before computing the peak amplitude; therefore, they are equal. **d,** Probability
314 density functions fitted using a Kernel distribution of the contralateral response for the treated groups
315 (Rd10 ET, Rd10 LT, and Rd10 ELT) compared to WT and Rd10 mice. **e,** Probability density functions
316 fitted with a Kernel distribution of the contralateral response for the sham-treated groups (Rd10 ES and
317 Rd10 ELS) mice compared to WT and Rd10 mice.

318 Finally, we further compared the scaled probability density functions (pdf, **Supplementary Fig. 3**) of
319 the VEP prominences in the treated (**Fig. 6d**) and sham-treated (**Fig. 6e**) mice to the ones of WT and
320 Rd10 mice. In WT mice, the pdf was broadly centred at 50 µV. All of the treated groups had a
321 distribution that appeared to be concentrated around 50 µV and narrower than the one of WT mice. In
322 contrast, sham-treated and control groups distributions are skewed towards 0, highlighting the higher
323 amount of non-responding mice.

15
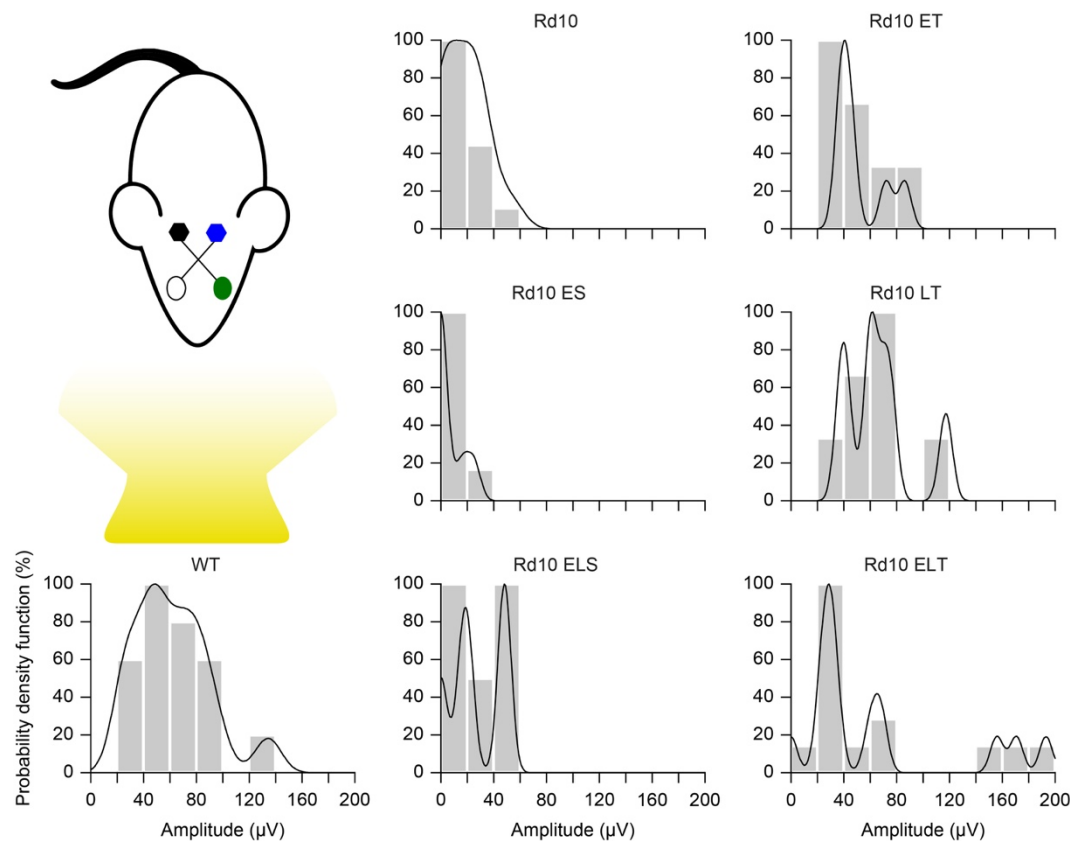
Supplementary Figure 3 | Probability density function. Each panel shows the histogram (20 µV bins) of the VEP peak amplitude and the fitted Kernel distribution for all the experimental groups. For treated (Rd10 ET, Rd10 LT, and Rd10 ELT) and sham treated (Rd10 ES and Rd10 ELS) mice, the data are from recordings in the cortex (black) contralateral to the treated eye (green).

Discussion

The eye is considered to be a preferential target for the delivery of gene therapies due to its accessibility and immune privilege(Sahel and Roska, 2012). Gene defects affecting photoreceptors cause the vast majority of IRDs; therefore, the development of neuroprotective, gene supplementation, and gene editing therapies has focused primarily on gene transfer to photoreceptors(Lipinski et al., 2015; Smith et al., 2012; Yu et al., 2017). While several retinal cell types can be successfully targeted by different viruses(Colella et al., 2009), the posterior segment of the eye, especially the photoreceptor layer, can be efficiently transduced only by Adeno Associated Viruses (AAVs)(Allocca et al., 2007). Unfortunately, the maximum cargo capacity of these vectors is around 4.7 kb, making them not suitable for the delivery of large genes. CRISPR/Cas9 plasmids are usually bigger than 5 kb and do not fit into AAVs. Hence, to deliver this gene editing tools, it is necessary to either combine more than one AAV

16

340 vector(Trapani, 2017; Trapani et al., 2014) or use other less safe viral vectors with larger cargo

341 capacity(Rossidis et al., 2018). A smaller Cas9 variant, delivered using AAVs, was recently used to

342 disrupt and thus inactivate the P23H mutated allele in a mouse model of dominant retinitis pigmentosa,

343 but the authors reported a poor cleavage efficiency(Giannelli et al., 2018). Moreover, even though

344 viruses represent the gold standard for gene delivery to the eye, their use does not cease to raise concerns

345 about immunogenicity, long-term safety, and limited possibility for repeated administration(Baum et

346 al., 2006; Thomas et al., 2003; Worgall et al., 2008; Yoshioka et al., 2006). Conversely, non-viral gene

347 delivery strategies(Al-Dosari and Gao, 2009; Niidome and Huang, 2002) permit the multiple

348 administration of large therapeutic agents using less immunogenic and toxic plasmid vectors, but the

349 resulting gene expression is often short-lived(Andrieu-Soler et al., 2007; Bainbridge et al., 2006; Han

350 et al., 2011). This is usually an unappealing characteristic for a clinical application, but it does not

351 represent a concern when editing tools need to be active only for a short period required to correct the

352 sequence of the gene of interest. Among the non-viral delivery strategies, electroporation is one of the

353 most efficient for the introduction of DNA into cells and holds a promising therapeutic

354 potential(Cancedda et al., 2013; Cwetsch et al., 2018; Gehl, 2003; dal Maschio et al., 2012;

355 Szczurkowska et al., 2013; 2016).

356 In fact, electroporation has been exploited for introducing genetic material and drugs in different tissues

357 and organs and for the treatment of cancer(Cwetsch et al., 2018; Gothelf et al., 2003; Lambricht et al.,

358 2015). According to *in vitro* reports(Hornstein et al., 2016), the size of the plasmid does not have any

359 impact on the transfection efficiency, making the technique suitable for the delivery of large genes that

360 would not fit into AAV viruses. Electroporation has been widely used to study the mouse retina

361 development(Matsuda and Cepko, 2004; 2007; 2008) but is still under investigation for therapeutic

362 purposes. The only reported use of electroporation on the human eye is in the human ciliary

363 muscle(Touchard et al., 2009). Albeit it has not yet been applied to the human retina, it has been shown

364 to successfully target different retinal cell types, both in young(Matsuda and Cepko, 2007; Wang et al.,

365 2014) and adult(Touchard et al., 2012) mice.

17

366   In our opinion, electroporation is an attractive alternative method for the delivery of large therapeutic

367   plasmids in the eye. Indeed, CRISPR/Cas9 constructs were also successfully delivered by

368   electroporation in photoreceptor cells to target and disrupt by NHEJ the rhodopsin mutated allele in

369   heterozygous P23H mice(Giannelli et al., 2018; Latella et al., 2016) and in S334ter rats, both model of

370   autosomal dominant retinitis pigmentosa(Bakondi et al., 2016). Nevertheless, loss of function mutations

371   (like the one affecting Rd10 mice) are more difficult to address since the faulty sequence has to be

372   actively edited by HDR to restore the correct gene product and not just disrupted as in the examples

373   cited above.

374   In this work, retinal electroporation was exploited to deliver a therapeutic DNA mixture to

375   photoreceptor cells. We treated Rd10 mice during photoreceptor development using a CRISPR/Cas9-

376   based gene editing strategy to prevent retinal degeneration and observed preservation of visual functions

377   *in vitro* and *in vivo*, in both subcortical visual-driven behavioural responses (optomotor reflex) and

378   cortical visual responses (VEP) until as late as P90. However, the visual acuity, measured with the

379   optomotor test, eventually declined at the postnatal day 90, even in treated mice. We hypothesise that,

380   since the coverage of the injection is not enough to edit the DNA of all the photoreceptor cells,

381   eventually, also the edited cells succumb to the adverse effect of pro-apoptotic factors released by the

382   non-edited dying cells. Multiple cycles of injections followed by electroporation could solve this issue

383   by allowing the gene editing of a higher number of photoreceptors, especially if performed during the

384   progenitor proliferation period. Notably, we have demonstrated that a repeated treatment (at P3 and P8)

385   is not detrimental for the mice. However, the mouse, especially the pup, is not an ideal model to test

386   this hypothesis, given the tiny size of the eyes: multiple injections and electroporation would damage

387   the eye excessively. Similarly, early intervention on new-born pups (P0-P1) could result in higher

388   editing efficiency.

389   In conclusion, we provide an example of how CRISPR/Cas9 gene editing can be coupled with

390   electroporation for therapeutic purpose, along with a discussion of the limitations that need to be

391   overcome to translate this approach to the clinics. Issues related to safety of retinal electroporation in

392   large animals, repeatability of the treatment, transfection efficiency, retinal coverage, gene expression

18

393 levels, and disease stage at the age of injection still need a careful investigation to improve the

394 therapeutic benefits of CRISPR/Cas9-based gene editing strategies. On the other hand, the ease of

395 design of the CRISPR/Cas9 gene editing systems makes them easily tailorable for several mutations in

396 perspective of a patient-specific therapy. This concept applies particularly when there are small

397 differences in the DNA sequence, as in the case of autosomal recessive mutations. Our non-viral

398 delivery approach has two main advantages compared to previous reports in small animal models in

399 which retinal degeneration was prevented by viral-mediated delivery of Cas9. First, in perspective of a

400 possible clinical application, it circumvents possible safety issues deriving from viral-based gene

401 therapy. Secondly, plasmid vector delivery by electroporation will result in transient expression of Cas9,

402 therefore limiting the possible occurrence of off-target activity of the nuclease after long-term

403 expression.

404

405 **Methods**

406 ***Construct Design and Cloning***. The online CRISPR Design Tool (http://tools.genome-

407 engineering.org) was used to design the gRNAs targeting the mouse gene *Pde6b* at the level of the

408 mutation C1678T. The sequence of the gene was used as input, and the first three best scoring gRNAs

409 were selected. gRNA #1 and gRNA #3 flanked the mutation C1678T (mapping respectively upstream

410 and downstream the mutation), while gRNA #2 and its Rd10-mutated counterpart gRNA #4 mapped on

411 the mutation. The gRNA sequences (#n) are the following: gRNA #1, gtggtaggtgattcttcgat; gRNA #2,

412 tgaagccgtggc**g**ccagttg; gRNA #3, tctgggctacattgaagccg; gRNA #4, tgaagccgtggc**a**ccagttg. The gRNA

413 #2 and #4 differ only for one base (in bold). The oligonucleotides to generate the gRNAs (Integrated

414 DNA Technologies) were annealed *in vitro* and cloned in the BbsI sites of the pSpCas9(BB)-2A-GFP

415 plasmid (#48138, Addgene). The original CBh promoter in pSpCas9(BB)-2A-GFP plasmid was then

416 replaced with the CAGGs promoter from pCAGGs–mCherry (#41583, Addgene). The obtained

417 pCAGGs-Cas9(BB)-2A-GFP-gRNA plasmid was subsequently used for the *in vitro* experiments. To

418 design the single-stranded oligodeoxynucleotide (ssODN) to use as repair templates, we took advantage

419 of a BanI restriction site in the target sequence to develop a screening assay that allowed us to

19

420 distinguish between the edited and the non-edited sequences. The BanI restriction site (GGYRCC,

421 where Y = C or T and R = A or G) maps just downstream to the C1678T mutation and is present both

422 in the WT (GGCGCC) and the Rd10 (GGTGCC) *Pde6b* sequence. We designed individual ssODN

423 repair templates for each gRNA (**Tab. 1**) in order to introduce a silent mutation in the corresponding

424 gRNA PAM sequence (NGG) to avoid Cas9 mediated re-processing of the edited DNA strand.

425 Moreover, the repair ssODNs (Integrated DNA Technologies, Ultramer^{TM} DNA oligo*)* were designed

426 to restore the codon coding for the Arginine (mutated into a Cystein in the Rd10 mice, R560C) and

427 concomitantly destroy the BanI restriction site (TGC to AGA). Since the gRNA #2 and #4 differ only

428 by one base, they share the same ssODN.

ssODN	gRNA	DNA sequence
1	1	Ccctctgattcatctagcccatccaatttacatacgtaccatgagtagggtaaacatggtctgggctacattgaagcc gtg**TCT**ccagtt**gtggtaggtgattcttcgat**at̲gctttgctgacagagaatagaaagcgcaccaagacctggg gagcagagtacatgtgggttctgagatccacatatgagcctacacagc
2	2 and 4	gctgtggtccttgccccagccctctgattcatctagcccatccaatttacatacgtaccatgagtagggtaaacatggt ctgggctacatt**gaagccgtgTCTccagttg**tg̲ataggtgattcttcgataggctttgctgacagagaatagaaa gcgcaccaagacctgggggagcagagtacatgtgggttctgagatcc
3	3	Agaagatagttagctgtggtccttgccccagccctctgattcatctagcccatccaatttacatacgtaccatgagta gggtaaacatgg**tctgggctacattgaagccg**tg**TCT**ccagttgtggtaggtgattcttcgataggctttgctga caggaatagaaagcgcaccaagacctgggggagcagagtacatgtgg

429 **Table 1. ssODNs coupled with each gRNA.** The sequences in bold represent the gRNAs and the ones

430 in bold capital letters represent the edited bases that restore the Arginine and delete the BanI restriction

431 site. The bases underlined are those mutated in the PAM sequence. The ssODNs are antisense to the

432 Pde6b sequence.

433 *N2A Cell Culture and Transfection*. Mouse N2A cells (ATCC® CCL-131™) were cultured in

434 Dulbecco's minimum essential medium (DMEM, Life Technologies) supplemented with 10 % foetal

435 calf serum (Life Technologies), 1 % L-glutamine, 100 U ml^{-1} penicillin, and 100 mg ml^{-1} streptomycin

436 (Biowhittaker-Lonza). Cells were maintained at 37 °C in a 5 % CO_2 humidified atmosphere. The cells

437   were transfected with Fugene 6 (Roche). The day before transfection 5 x 10^5 N2A cells were plated on

438   6 cm plates. The medium was replaced with fresh medium 1 h before the transfection. The DNA/Fugene

439   mix (ratio 1:2) was prepared in Optimem medium (Life Technologies). N2A cells were co-transfected

440   with 1.5 µg of pCAGGs-Cas9(BB)-2A-GFP-gRNA #(n) and 2.2 µg of the associated repair template.

441   Cells plated on different wells were transfected with different gRNAs. Cells were incubated at 37 °C in

442   a 5 % CO_2 humidified atmosphere for 48 h following transfection, then detached using Trypsin-EDTA

443   0.25 % (Sigma-Aldrich), and prepared for FAC-sorting.

444   ***Preparation of Neurospheres and Nucleofection***. Primary cultures of NSC were prepared from WT

445   and Rd10 mice(Pacey et al., 2006). P2 mice were decapitated, and the brain was removed from the

446   skull. The cortex and the hippocampus were isolated and cut in small cubes in the tissue dissection

447   solution (in mM): 124 NaCl, 5 KCl, 3.2 $MgCl_2$, 26 $NaHCO_3$, 10 glucose, and 0.1 $CaCl_2$ (Sigma-

448   Aldrich). An enzyme mix was dissolved in 30 ml of tissue dissection solution and added: trypsin 0.04

449   g, Type 1-S Hyaluronidase 0.02 g, and kynurenic acid 0.004 g (Sigma-Aldrich). The tissue was

450   incubated for 40 min in a water bath at 37 °C and triturated with a Pasteur pipette every 20 min. After

451   centrifugation, the enzyme mix was removed and the trypsin inhibitor (Sigma-Aldrich), dissolved in

452   serum-free medium (SFM) at the concentration of 1 mg ml^{-1}, was added. The tissue was then triturated

453   and incubated in the water bath for an additional 10 min. After centrifugation, the tissue was

454   resuspended in SFM containing: DMEM/F12 (Life Technologies), 20 ng ml^{-1} EGF (Peprotech), 20 ng

455   ml^{-1} FGF (Peprotech), 2 % v/v B-27 (Life Technologies), 1.83 µg ml^{-1} Heparin (Sigma-Aldrich), 1 mM

456   Putrescine (Sigma-Aldrich), 2 µM Progesterone (Sigma-Aldrich), 10 µg ml^{-1} ITSS (Sigma-Aldrich), 6

457   mg ml^{-1} glucose (Sigma-Aldrich), and 1 % Pen/Strep (Life Technologies). Then, the tissue was

458   triturated to obtain a single-cell solution. The cells were counted with the vital dye Trypan blue (Sigma-

459   Aldrich) and then plated at 100.000 cells in each well of a 12-well non-coated plate. We obtained

460   neurospheres that were maintained in SFM at 37 °C in a 5 % CO_2 humidified atmosphere and passed

461   1:3 for three times a week. After 3 to 4 passages cell were electroporated *via* Nucleofection with the

462   AMAXA nucleofection device (LONZA). The Neurospheres were dissociated with Accutase (Sigma-

463   Aldrich) and 5 x 10^6 NSCs were electroporated with 2 µg of pCAGGs-Cas9(BB)-2A-GFP-gRNA and

21

464   2 μl of repair template (10 μM) following the protocol suggested by the manufacturer. Cells were then

465   incubated at 37 °C in a 5 % CO_2 humidified atmosphere for 30 hours, dissociated with Accutase, and

466   GFP-positive cells isolated by FACS.

467   ***Restriction analysis***. Cells in Hibernate-A medium were filtered (Life Technologies) and FACS-

468   isolated with a FACSAria (BD-Biosciences). GFP positive cells were collected in a tube containing

469   PBS + FBS 2 %. The gDNA of the sorted cells (both N2A and NSCs) was extracted with the Genomic

470   DNA™ - Tissue MiniPrep kit (Zymo Research) following the protocol of the manufacturer for cell

471   suspensions. The DNA was eluted in 30 μl of DNAse-free water and concentration measured at 260 nm

472   with an ND1000 Nanodrop spectrophotometer (Thermo Scientific). 125 ng of purified gDNA was used

473   for PCR amplification. The following primers (Sigma-Aldrich), mapping outside the ssODN sequence

474   were used to amplify a region of ≈ 700 bps containing the edited region of the *Pde6b* gene:

475   tttctgctcacaggccacat (forward) and gctccagaaggcagtggtta (reverse). The DNA fragment obtained by

476   amplification was purified with the PCR purification kit (QIAGEN) and quantified as above. For the

477   restriction analysis of PCR products, 300 ng of DNA was digested with 5 units of BanI enzyme for 1

478   hour in 25 μl total reaction volume. The digestion of the PCR fragment obtained amplifying unedited

479   gDNA with the BanI restriction enzyme generated two fragments of 470 and 230 bps respectively that

480   were resolved on 2 % agarose gel. The PCR fragments obtained amplifying the edited gDNA could not

481   be digested by the BanI enzyme, thus leaving the undigested 700 bps fragment on an agarose gel. The

482   optical density of the 700-bps band was measured using the gel tool of ImageJ.

483   ***Plasmids and DNA preparation for in vivo delivery***. The nanoplasmids expressing eGFP and Cas9/GFP

484   were purchased from Nature Technology, and the template repair was purchased from Integrated DNA

485   Technologies. The gRNA was cloned into the pSPgRNA plasmid (#47108, Addgene). All the

486   components used for the *in vivo* experiments are specified in **Table 2**.

Component	Name	Length	Supplier
eGFP plasmid	NTC9385R-eGFP	2391 bp	Nature Technology
Cas9 plasmid	NTC9385R-CAGCas9-T2A-GFP	6500 bp	Nature Technology

gRNA plasmid	pSPgRNA	3000 bp	Addgene
Repair template	ssODN	200 nucleotides	IDT

Table 2. Full name, size, and origin of all the components used in the in vivo experiments. The concentrations were adjusted in order to have the same number of copies of guide-coding and Cas9-coding plasmids, taking into account the relative number of base pairs. The repair ssODN concentration is similar to what previously described for CRISPR-Cas9 editing systems.

The following are the specific solutions used for each experiment (all of them were prepared in PBS with the addition of 0.1 % Fast green for the visualisation of the injection):

- eGFP preparation: eGFP-coding plasmid (1 µg µl^{-1}).

- Cas9 preparation: Cas9-coding plasmid (1 µg µl^{-1}) + gRNA-coding plasmid (0.45 µg µl^{-1}) + repair ssODN (2 µl µg of Cas9^{-1}).

- Sham preparation: Cas9-coding plasmid (1 µg µl^{-1}) + repair ssODN (2 µl µg of Cas9^{-1}).

- Cas9 + eGFP (1.5:1) preparation: Cas9-coding plasmid (1.5 µg µl^{-1}) + gRNA-coding plasmid (0.8 µg µl^{-1}) + eGFP-coding plasmid (0.9 µg µl^{-1}) + repair ssODN (2 µl µg of Cas9^{-1}).

Animal handling. Animal experiments were performed according to the animal authorizations VD3044 issued by the Service de la consommation et des Affaires vétérinaires (SCAV) of the Canton de Vaud (Switzerland), GE3217 issued by the Département de l'emploi, des affaires sociales et de la santé (DEAS), Direction générale de la santé of the Republique et Canton de Genève (Switzerland), and 726/2015-PR issued by the Italian Ministry of Health. Male and female mice pups at P3 and P8 and adult mice at 1, 2, and 3 months of age from a homozygous colony of B6.CXB1-*Pde6b^{rd10}*/J mice (The Jackson Laboratory) were used for the experiments. C57BL/6J mice (Charles River) were used as control group. All animals were kept in a 12 h day/night cycle with access to food and water ad libitum. All pups were kept with the mother until weaning, except for the time necessary to perform the subretinal injection. All the experiments were carried out during the day cycle.

Subretinal injection and electroporation. Subretinal injections were performed in mice pups at P3, P8, or both. The pups were anaesthetised using isoflurane (0.8-1.5 l min^{-1} at 3 %) in an induction box, then

23

511 placed onto a sterile paper towel under a microscope; the anaesthesia was maintained with isoflurane

512 (0.8-1.5 l min^{-1} at 2 %), and the temperature was maintained at 37 °C with a heating pad. The skin over

513 the eyelid was disinfected with Betadine, and a sterile 30-G needle was used to cut the skin on the mark

514 of the future eyelid aperture. The skin was gently pushed to the side with a pair of sterile forceps to

515 expose the eyeball. A glass capillary (ORIGIO) backfilled with the DNA solution was insert into the

516 subretinal space, maintaining a 45° inclination to the surface of the eye. The DNA solution was then

517 injected into the subretinal space for 3 seconds at 300 hPa using an automatic injector (Eppendorf). Two

518 injections were performed in the following directions: dorsal to nasal and ventral to nasal. Immediately

519 after the DNA injection, an electric field was applied to the area using a P5 tweezer electrode (Sonidel)

520 pre-soaked in PBS. The positive terminal was attached to the sclera of the injected eye, while the other

521 side of the tweezer (negative terminal) was placed on the not-injected eye. The pulses were delivered

522 using a CUY21SC electroporator (Sonidel). A conductive gel was placed between the electrode plate

523 and the eye to maximise the conductivity and minimise burns on the cornea. Two square pulses of 5 ms

524 at 100 V were applied with 0.1 Hz frequency (poring pulses), followed by five pulses of 50 ms at 30 V

525 with 1 Hz frequency (transfer pulses). After the procedure, the eyelid was closed gently with a cotton

526 swab, and the pup was placed onto a heating pad at 37 °C until fully recovered, then returned to the

527 mother. In all the groups the injection was performed unilaterally in order to keep the other eye as an

528 internal control. The pups were treated daily during the first-week post-surgery with Tobradex Eye

529 Drops (tobramycin 0.3 % and dexamethasone 0.1 %) on the operated eye.

530 ***Retina sections and wholemounts***. Mice for retina sections and wholemounts were electroporated at

531 P3 or P8 with the eGFP construct. After euthanasia by CO_2 inhalation, the eyes of the mice were

532 extracted from the ocular cavity using forceps, washed in PBS, and fixed in 4 % PFA overnight. For

533 wholemount preparation, the retina was extracted and cut in 4 points in order to flat it on a microscope

534 slide. For section preparation, the samples were cryoprotected in sucrose 30 % and frozen in optimal

535 cutting temperature compound (Tissue-Tek®). 20 μm thick sections of the retina were obtained using

536 a Histocom cryostat (Thermo Scientific) and placed on microscope slides. The sections and the

537 wholemounts were washed in PBS, permeabilised with PBS + Triton 0.1 % (Sigma-Aldrich),

24

538   counterstained with DAPI 1:300 (Sigma-Aldrich), and mounted for imaging with Fluoromount (Sigma-

539   Aldrich).

540   ***Droplet-digital PCR***. The eyes of P6 mice electroporated at P3 were enucleated, and the retina was

541   immediately isolated in ice-cold PBS and quickly inspected under a fluorescence microscope to verify

542   eGFP expression. The gDNA was extracted using the Genomic DNA™ - Tissue MiniPrep kit (Zymo

543   Research) following the protocol of the manufacturer for solid tissues. The DNA was eluted in 30 µl of

544   DNase-free water. To avoid possible false-positive signals in ddPCR from unintegrated ssODN repair

545   template, we optimised a nested-ddPCR assay. We first pre-amplified from extracted gDNA by

546   conventional PCR a fragment of ≈700 bps containing the edited region of the *Pde6b* gene with primers

547   mapping outside the ssODN sequence (same as for the BanI restriction assay). The amplified DNA

548   fragment was purified and quantified as above. Next 2.5 fg of the purified template (corresponding to

549   ≈3500 copies of target DNA) was used in the ddPCR assay with internal primers (Fwd:

550   CAGCAAAGCCTATCGAAGAATCA; Rev: CATGGTCTGGGCTACATTGAAG) and detected with

551   an edited-specific TaqMan® probe (FAM- TATCACAACTGGAGACAC-MGB) and an unedited-

552   specific TaqMan® probe (VIC-TACCACAACTGGTGCCA-MGB). Reactions were assembled with

553   ddPCR™ Supermix for Probes (Bio-Rad Laboratories) and partitioned into nanoliter-sized droplets

554   with QX200 Droplet Generator (Bio-Rad Laboratories). After PCR thermal cycling, droplets for each

555   sample were individually read on a QX200 Droplet Reader (Bio-Rad Laboratories) and assigned as

556   positive or negative based on fluorescence amplitude.

557   ***Recordings of microelectroretinograms***. P60 mice electroporated at P3 were dark-adapted overnight

558   before tissue collection. All procedures were performed under dim red light. Retinas were explanted

559   after euthanasia by intraperitoneal injection of sodium pentobarbital (150 mg kg^{-1}). The retinas were

560   dissected in carboxygenated (95 % O_2 and 5 % CO_2) Ames' medium (A1420, Sigma-Aldrich). After

561   dissection of the sclera, the retina was detached from the pigment epithelium, and the vitreous humour

562   was removed. The retina was then cut into pieces (approximately 5 mm^2), attached to a filter paper, and

563   transferred onto the MEA (256MEA200/30iR-ITO; Multi Channel Systems) with the ganglion cell layer

564   facing the electrodes. Explanted retinas were continuously superfused with carboxygenated Ames's

25

565   medium at 32 °C. Data acquisition, amplification, and digitalisation were performed with a recording

566   system (USB-MEA256-System; Multi Channel Systems) placed on the stage of an inverted Ti-E

567   microscope (Nikon Instruments). The microscope was equipped with a dichroic filter (FF875-Di01-

568   25x36; Semrock) and a 4x objective (diameter of the illumination spot 5.5 mm; CFI Plan Apochromat

569   Lambda). Light stimuli were provided by an attached Spectra X system (Emission filter 560/32;

570   Lumencor). Ten consecutive pulses of 4 ms and 0.5 mW mm^{-2} were delivered at a repetition rate of 1

571   Hz. The extracellularly recorded signals were digitalised and stored for offline analysis. Data filtering

572   and spike sorting were performed using the MC_Rack software (Multi Channel Systems). The presence

573   of spontaneous spiking activity was assessed (filter 300-3000 Hz, sampling rate of 25 kHz) to ensure

574   the viability of the retinal explant. Only retinas showing spontaneous activity in at least one channel

575   when placed on the MEAs were selected for recordings, and each responding channel was treated as an

576   independent unit. To detect μERGs, the signal was filtered from 0.5 to 100 Hz and digitalised at 10

577   kHz. The prominence of the μERG a-wave was computed for each channel in MATLAB (MathWorks).

578   ***Measurement of the visual acuity***. The Optomotor system (Cerebral Mechanics) was used for the

579   measurement of the visual acuity. Control and treated mice were habituated for 5 min placing them in

580   the centre of the virtual arena the day before the beginning of the test. The day of the test, each mouse

581   was placed on the platform, and the program started. The mouse in the arena was presented with a

582   grating stimulus rotating in either direction, and the operator had to decide if the mouse was tracking or

583   not the rotating stimulus with a movement of the head in the same direction of the rotation. The program

584   uses a built-in algorithm based on a staircase method to evaluate the visual threshold of the two eyes

585   independently. The performance of any single mouse was assessed during three subsequent days, and

586   the resulting average was considered the value of the mouse visual threshold. Mice were tested at P30,

587   P60, and P90.

588   ***Electrode implantation and recording of visually evoked potentials***. Before the surgical procedures

589   and the recording sessions, the mice were anaesthetised with isoflurane (0.8-1.5 l min^{-1} at 4 % for

590   induction and 0.8-1.5 l min^{-1} at 1.5 % for maintenance). Analgesia was administered by subcutaneous

591   injection of Buprenorphine (Temgesic, 0.1 mg kg^{-1}) followed by subcutaneous injection of a mix

26

592   composed by lidocaine (6 mg kg^{-1}) and bupivacaine (2.5 mg kg^{-1}) with a 1:1 ratio. The depth of

593   anaesthesia was assessed with the pedal reflex, and artificial tears were used to prevent the eyes from

594   drying. The temperature was maintained at 37 °C with a heating pad during both surgical and recording

595   sessions. For electrode implantation, anaesthetised P60 mice mounted on a stereotaxic apparatus. The

596   skull was exposed for the visualisation of lambda, and the skin was pulled on the side. Two screw

597   electrodes were implanted 3 mm lateral to lambda over the left and right visual cortices. A reference

598   electrode was placed in the rostral side of the cranium, outside of the visual cortex. The electrodes were

599   fixed using dental cement. The screws were then left in place for 30 more days. The surgery was

600   performed in advance in order to let the electrodes to stabilise. For recordings, all the procedures were

601   performed under dim red light. P90 mice were dark-adapted overnight, anaesthetised, and mounted on

602   a stereotaxic frame. The pupils were dilated with a drop of Atropine 1 %, and a needle electrode was

603   placed subcutaneously in the dorsal area near the tail as ground. The recordings were acquired

604   simultaneously in two channels connected to the two electrodes implanted on both visual cortices. Three

605   light flashes (4 ms, 10 cd s m^{-2}, interleaved by 2 min) were delivered with a Ganzfeld stimulator

606   (BM6007IL, Biomedica Mangoni) positioned close to the mice and the corresponding visually evoked

607   cortical potentials were amplified, filtered (0.1 – 500 Hz), and digitalized for 1000 ms (50 ms pre-

608   stimulus and 950 ms post-stimulus) at 2 kHz (BM623, Biomedica Mangoni). The data were analysed

609   using MATLAB (MathWorks).

610   ***Statistical analysis and graphical representation***. Statistical analysis and graphical representation were

611   performed with Prism (GraphPad Software Inc.). The normality test (D'Agostino & Pearson omnibus

612   normality test) was performed in each dataset to justify the use of a parametric (t-test and One-Way

613   ANOVA) or non-parametric (Kruskal-Wallis and Mann-Whitney) test. The fitting of the VEPs was

614   performed with the non-parametric Kernel distribution in MATLAB. In each figure p-values were

615   represented as: * $p < 0.05$, ** $p < 0.01$, *** $p < 0.001$, and **** $p < 0.0001$.

616   ***Data availability***. The authors declare that all other relevant data supporting the findings of the study

617   are available in this article and its Supplementary Information file. Access to our raw data can be

618   obtained from the corresponding author upon reasonable request.

Acknowledgements

Competing interests

The authors declare no competing financial interest.

Author Contributions

P.V. performed all the experiments and wrote the manuscript. L.E.P. designed the gene editing strategy, generated the plasmids, and performed in vitro validation of the plasmids. N.A.L.C. performed experiments with explanted retinas. T.M. contributed to in vivo electrophysiology. M.P. contributed to the setting of pilot behavioural experiments. A.C. designed the study, designed the gene editing and screening strategies, performed the ddPCR and wrote the manuscript. L.C. designed the study. D.G. designed the study, led the whole project, and wrote the manuscript. All the authors read, edited, and accepted the manuscript.

References

Al-Dosari, M.S., and Gao, X. (2009). Nonviral Gene Delivery: Principle, Limitations, and Recent Progress. The AAPS Journal *11*, 671–681.

644   Allocca, M., Mussolino, C., Garcia-Hoyos, M., Sanges, D., Iodice, C., Petrillo, M., Vandenberghe,

645   L.H., Wilson, J.M., Marigo, V., Surace, E.M., et al. (2007). Novel Adeno-Associated Virus Serotypes

646   Efficiently Transduce Murine Photoreceptors ▿ . J Virol *81*, 11372–11380.

647

648   Andrieu-Soler, C., Halhal, M., and Boatright, J. (2007). Single-stranded oligonucleotide-mediated in

649   vivo gene repair in the rd1 retina.

650

651   Auricchio, A., Smith, A.J., and Ali, R.R. (2017). The Future Looks Brighter After 25 Years of Retinal

652   Gene Therapy. Hum Gene Ther *28*, 982–987.

653

654   Bainbridge, J., Tan, M., and Ali, R. (2006). Gene therapy progress and prospects: the eye. Gene Ther

655   *13*, 3302812.

656

657   Bakondi, B., Lv, W., Lu, B., Jones, M.K., Tsai, Y., Kim, K.J., Levy, R., Akhtar, A., Breunig, J.J.,

658   Svendsen, C.N., et al. (2016). In Vivo CRISPR/Cas9 Gene Editing Corrects Retinal Dystrophy in the

659   S334ter-3 Rat Model of Autosomal Dominant Retinitis Pigmentosa. Molecular Therapy *24*, 556–563.

660

661   Baum, C., Kustikova, O., Modlich, U., Li, Z., and Fehse, B. (2006). Mutagenesis and oncogenesis by

662   chromosomal insertion of gene transfer vectors. Human Gene Therapy *17*, 253–263.

663

664   Bennett, J., Tanabe, T., Sun, D., Zeng, Y., Kjeldbye, H., Gouras, P., and Maguire, A. (1996).

665   Photoreceptor cell rescue in retinal degeneration (rd) mice by in vivo gene therapy. Nature Medicine

666   *2*, 649–654.

667

668   Bureau, M.F., Gehl, J., Deleuze, V., Mir, L.M., and Scherman, D. (2000). Importance of association

669   between permeabilization and electrophoretic forces for intramuscular DNA electrotransfer.

670   Biochimica Et Biophysica Acta Bba - Gen Subj *1474*, 353–359.

671

672   Cancedda, L., Szczurkowska, J., Cwetsch, A.W., dal Maschio, M., Ghezzi, D., Ratto, G., and

673   Cancedda, L. (2013). High-performance and reliable site-directed in vivo genetic manipulation of

674   mouse and rat brain by in utero electroporation with a triple-electrode probe. Protocol Exchange.

675

676   Chang, B., Hawes, N.L., Hurd, R.E., Davisson, M.T., Nusinowitz, S., and Heckenlively, J.R. (2002).

677   Retinal degeneration mutants in the mouse. Vision Research *42*.

678

679   Chang, B., Hawes, N.L., Pardue, M.T., German, A.M., Hurd, R.E., Davisson, M.T., Nusinowitz, S.,

680   Rengarajan, K., Boyd, A.P., Sidney, S.S., et al. (2007). Two mouse retinal degenerations caused by

681   missense mutations in the β-subunit of rod cGMP phosphodiesterase gene. Vision Research *47*.

682

683   Colella, P., Cotugno, G., and Auricchio, A. (2009). Ocular gene therapy: current progress and future

684   prospects. Trends in Molecular Medicine *15*, 23–31.

685

686   Coleman, J.E., Law, K., and Bear, M.F. (2009). Anatomical origins of ocular dominance in mouse

687   primary visual cortex. Neuroscience *161*, 561–571.

688

689   Cong, L., Ran, A.F., Cox, D., Lin, S., Barretto, R., Habib, N., Hsu, P.D., Wu, X., Jiang, W.,

690   Marraffini, L.A., et al. (2013). Multiplex Genome Engineering Using CRISPR/Cas Systems. Science

691   *339*, 819–823.

692

693   Cwetsch, A.W., Pinto, B., Savardi, A., and Cancedda, L. (2018). In vivo methods for acute

694   modulation of gene expression in the central nervous system. Prog Neurobiol *168*, 69–85.

695

696   DANCIGER, M., JOHN, E., GAO, Y.Q., ZHAO, D.Y., HECKENLIVELY, J.R., JACOBSON, S.G.,

697   and FARBER, D.B. (1995). Mutations in the PDE6B Gene in Autosomal Recessive Retinitis

698   Pigmentosa. Genomics *30*, 1–7.

699

700   DOUGLAS, R.M., ALAM, N.M., SILVER, B.D., MCGILL, T.J., TSCHETTER, W.W., and

701   PRUSKY, G.T. (2005). Independent visual threshold measurements in the two eyes of freely moving

702   rats and mice using a virtual-reality optokinetic system. Visual Neurosci *22*, 677–684.

703

704   Ferrari, S., Iorio, E., Barbaro, V., Ponzin, D., Sorrentino, F.S., and Parmeggiani, F. (2011). Retinitis

705   Pigmentosa: Genes and Disease Mechanisms. Curr Genomics *12*, 238–249.

706

707   Gargini, C., Terzibasi, E., Mazzoni, F., and Strettoi, E. (2007). Retinal organization in the retinal

708   degeneration 10 (rd10) mutant mouse: A morphological and ERG study. J Comp Neurol *500*, 222–

709   238.

710

711   Gehl, J. (2003). Electroporation: theory and methods, perspectives for drug delivery, gene therapy and

712   research. Acta Physiol Scand *177*, 437–447.

713

714   Giannelli, S.G., Luoni, M., Castoldi, V., Massimino, L., Cabassi, T., Angeloni, D., Demontis, G.,

715   Leocani, L., Andreazzoli, M., and Broccoli, V. (2018). Cas9/sgRNA selective targeting of the P23H

716   Rhodopsin mutant allele for treating retinitis pigmentosa by intravitreal AAV9.PHP.B-based delivery.

717   Hum Mol Genet *27*, 761–779.

718

719   Gothelf, A., Mir, L.M., and Gehl, J. (2003). Electrochemotherapy: results of cancer treatment using

720   enhanced delivery of bleomycin by electroporation. Cancer Treat Rev *29*, 371–387.

721

722   Han, Z., Conley, S.M., and Naash, M.I. (2011). AAV and compacted DNA nanoparticles for the

723   treatment of retinal disorders: challenges and future prospects. Investigative Ophthalmology & Visual

724   Science *52*, 3051–3059.

725

726   Heidenreich, M., and Zhang, F. (2016). Applications of CRISPR-Cas systems in neuroscience. Nature

727   Reviews. Neuroscence *17*, 36–44.

728

729   Hornstein, B.D., Roman, D., Arévalo-Soliz, L.M., Engevik, M.A., and Zechiedrich, L. (2016). Effects

730   of Circular DNA Length on Transfection Efficiency by Electroporation into HeLa Cells. Plos One *11*,

731   e0167537.

732

733   Jae, S.A., Ahn, K., Kim, J., Seo, J., Kim, H., and Goo, Y. (2013). Electrophysiological and Histologic

734   Evaluation of the Time Course of Retinal Degeneration in the rd10 Mouse Model of Retinitis

735   Pigmentosa. Korean J Physiology Pharmacol Official J Korean Physiological Soc Korean Soc

736   Pharmacol *17*, 229–235.

737

738   Jomary, C., Vincent, K., Grist, J., Neal, M., and Jones, S. (1997). Rescue of photoreceptor function by

739   AAV-mediated gene transfer in a mouse model of inherited retinal degeneration. Gene Ther *4*,

740   3300440.

741

742   Lambricht, L., Lopes, A., Kos, S., Sersa, G., Préat, V., and Vandermeulen, G. (2015). Clinical

743   potential of electroporation for gene therapy and DNA vaccine delivery. Expert Opin Drug Del *13*,

744   295–310.

745

746   Latella, M., Salvo, M., Cocchiarella, F., Benati, D., Grisendi, G., Comitato, A., Marigo, V., and

747   Recchia, A. (2016). In vivo Editing of the Human Mutant Rhodopsin Gene by Electroporation of

748   Plasmid-based CRISPR/Cas9 in the Mouse Retina. Mol Ther - Nucleic Acids *5*, e389.

749

750   Lipinski, D.M., Barnard, A.R., Singh, M.S., Martin, C., Lee, E.J., Davies, W.I., and MacLaren, R.E.

751   (2015). CNTF Gene Therapy Confers Lifelong Neuroprotection in a Mouse Model of Human

752   Retinitis Pigmentosa. Mol Ther *23*, 1308–1319.

753

754   MacLaren, R., Pearson, R., MacNeil, A., Douglas, R., Salt, T., Akimoto, M., Swaroop, A., Sowden,

755   J., and Ali, R. (2006). Retinal repair by transplantation of photoreceptor precursors. Nature *444*, 203–

756   207.

757

758   dal Maschio, M., Ghezzi, D., Bony, G., Alabastri, A., Deidda, G., Brondi, M., Sato, S.S., Zaccaria,

759   R.P., Fabrizio, E., Ratto, G.M., et al. (2012). High-performance and site-directed in utero

760   electroporation by a triple-electrode probe. Nature Communications *3*, 960.

761

762   Matsuda, T., and Cepko, C.L. (2004). Electroporation and RNA interference in the rodent retina in

763   vivo and in vitro. Proceedings of the National Academy of Sciences of the United States of America

764   *101*, 16–22.

765

766   Matsuda, T., and Cepko, C.L. (2007). Controlled expression of transgenes introduced by in vivo

767   electroporation. Proceedings of the National Academy of Sciences *104*, 1027–1032.

768

769   Matsuda, T., and Cepko, C.L. (2008). Analysis of Gene Function in the Retina. Methods in Molecular

770   Biology (Clifton, N.J.) *423*, 259–278.

771

772   McLaughlin, M., Ehrhart, T., Berson, E., and Dryja, T. (1995). Mutation spectrum of the gene

773   encoding the beta subunit of rod phosphodiesterase among patients with autosomal recessive retinitis

774   pigmentosa. Proceedings of the National Academy of Sciences *92*, 3249–3253.

775

776   de Melo, J., and Blackshaw, S. (2011). In vivo electroporation of developing mouse retina. Journal of

777   Visualized Experiments : JoVE.

778

779   Mohand-Said, S., Hicks, D., Dreyfus, H., and Sahel, J. (2000). Selective Transplantation of Rods

780   Delays Cone Loss in a Retinitis Pigmentosa Model. Arch Ophthalmol-Chic *118*, 807–811.

781

782   Narayan, D.S., Wood, J.P., Chidlow, G., and Casson, R.J. (2016). A review of the mechanisms of

783   cone degeneration in retinitis pigmentosa. Acta Ophthalmol *94*, 748–754.

784

785   Niidome, T., and Huang, L. (2002). Gene therapy progress and prospects: nonviral vectors. Gene

786   Therapy *9*, 1647–1652.

787

788   Pacey, L., Stead, S., Gleave, J., Tomczyk, K., and Doering, L. (2006). Neural Stem Cell Culture:

789   Neurosphere generation, microscopical analysis and cryopreservation. Protoc Exch.

790

791   Pang, J., Boye, S.L., Kumar, A., Dinculescu, A., Deng, W., Li, J., Li, Q., Rani, A., Foster, T.C.,

792   Chang, B., et al. (2008). AAV-Mediated Gene Therapy for Retinal Degeneration in the rd10 Mouse

793   Containing a Recessive PDEβ Mutation. Investigative Ophthalmology & Visual Science.

794

795   Pang, -J J, Lei, L., Dai, X., Shi, W., Liu, X., Dinculescu, A., and well, J. (2012). AAV-Mediated Gene

796   Therapy in Mouse Models of Recessive Retinal Degeneration. Curr Mol Med *12*, 316–330.

797

798   Pennesi, M.E., Michaels, K.V., Magee, S.S., Maricle, A., Davin, S.P., Garg, A.K., Gale, M.J., Tu,

799   D.C., Wen, Y., Erker, L.R., et al. (2012). Long-Term Characterization of Retinal Degeneration in rd1

800   and rd10 Mice Using Spectral Domain Optical Coherence TomographySD-OCT Imaging of rd1 and

801   rd10 Mice. Investigative Ophthalmology & Visual Science *53*, 4644–4656.

802

803   Prusky, G.T., Alam, N.M., Beekman, S., and uglas, R. (2004). Rapid Quantification of Adult and

804   Developing Mouse Spatial Vision Using a Virtual Optomotor System. Investigative Ophthalmology

805   & Visual Science *45*, 4611–4616.

806

807   Ran, A.F., Hsu, P.D., Wright, J., Agarwala, V., Scott, D.A., and Zhang, F. (2013). Genome

808   engineering using the CRISPR-Cas9 system. Nature Protocols *8*, 2281–2308.

809

810   Rossidis, A.C., Stratigis, J.D., Chadwick, A.C., Hartman, H.A., Ahn, N.J., Li, H., Singh, K., Coons,

811   B.E., Li, L., Lv, W., et al. (2018). In utero CRISPR-mediated therapeutic editing of metabolic genes.

812   Nat Med *24*, 1513–1518.

813

814   Sahel, J.-A., and Roska, B. (2012). Gene Therapy for Blindness. Annual Review of Neuroscience *36*,

815   467–488.

816

817   Saleh-Gohari, N., and Helleday, T. (2004). Conservative homologous recombination preferentially

818   repairs DNA double-strand breaks in the S phase of the cell cycle in human cells. Nucleic Acids Res

819   *32*, 3683–3688.

820

821   Smith, A.J., Bainbridge, J.W., and Ali, R.R. (2012). Gene supplementation therapy for recessive

822   forms of inherited retinal dystrophies. Gene Therapy *19*, 154–161.

823

824   Stasheff, S.F., Shankar, M., and Andrews, M.P. (2011). Developmental time course distinguishes

825   changes in spontaneous and light-evoked retinal ganglion cell activity in rd1 and rd10 mice. Journal

826   of Neurophysiology *105*, 3002–3009.

827

828   Szczurkowska, J., dal Maschio, M., Cwetsch, A.W., Ghezzi, D., Bony, G., Alabastri, A., Zaccaria,

829   R.P., di Fabrizio, E., Ratto, G.M., and Cancedda, L. (2013). Increased performance in genetic

830   manipulation by modeling the dielectric properties of the rodent brain. Conference Proceedings : ...

831   Annual International Conference of the IEEE Engineering in Medicine and Biology Society. IEEE

832   Engineering in Medicine and Biology Society. Annual Conference *2013*, 1615–1618.

833

834   Szczurkowska, J., Cwetsch, A.W., dal Maschio, M., Ghezzi, D., Ratto, G., and Cancedda, L. (2016).

835   Targeted in vivo genetic manipulation of the mouse or rat brain by in utero electroporation with a

836   triple-electrode probe. Nature Protocols *11*, 399–412.

837

838   Thomas, C.E., Ehrhardt, A., and Kay, M.A. (2003). Progress and problems with the use of viral

35

839 vectors for gene therapy. Nat Rev Genet *4*, 346–358.

840

841 Touchard, E., Bloquel, C., Bigey, P., Kowalczuk, L., Kowalczuc, L., Jonet, L., Thillaye-Goldenberg,

842 B., Naud, M.-C.C., Scherman, D., de Kozak, Y., et al. (2009). Effects of ciliary muscle plasmid

843 electrotransfer of TNF-alpha soluble receptor variants in experimental uveitis. Gene Therapy *16*, 862–

844 873.

845

846 Touchard, E., Berdugo, M., Bigey, P., Sanharawi, M., Savoldelli, M., Naud, M.-C.C., Jeanny, J.-C.C.,

847 and Behar-Cohen, F. (2012). Suprachoroidal electrotransfer: a nonviral gene delivery method to

848 transfect the choroid and the retina without detaching the retina. Molecular Therapy : The Journal of

849 the American Society of Gene Therapy *20*, 1559–1570.

850

851 Trapani, I. (2017). Retinal Gene Therapy, Methods and Protocols. Methods Mol Biology Clifton N J

852 *1715*, 153–175.

853

854 Trapani, I., Colella, P., Sommella, A., Iodice, C., Cesi, G., Simone, S., Marrocco, E., Rossi, S., Giunti,

855 M., Palfi, A., et al. (2014). Effective delivery of large genes to the retina by dual AAV vectors.

856 EMBO Molecular Medicine.

857

858 Tucker, B.A., Park, I.-H., Qi, S.D., Klassen, H.J., Jiang, C., Yao, J., Redenti, S., Daley, G.Q., and

859 Young, M.J. (2011). Transplantation of Adult Mouse iPS Cell-Derived Photoreceptor Precursors

860 Restores Retinal Structure and Function in Degenerative Mice. Plos One *6*, e18992.

861

862 Ulshafer, R., Garcia, C., and Hollyfield, J. (1980). Sensitivity of photoreceptors to elevated levels of

863 cGMP in the human retina. Invest Ophth Vis Sci *19*, 1236–1241.

864

865 Wang, S., Sengel, C., Emerson, M.M., and Cepko, C.L. (2014). A gene regulatory network controls

866 the binary fate decision of rod and bipolar cells in the vertebrate retina. Developmental Cell *30*, 513–

867   527.

868

869   Worgall, S., Sondhi, D., Hackett, N.R., Kosofsky, B., Kekatpure, M.V., Neyzi, N., Dyke, J.P., Ballon,

870   D., Heier, L., Greenwald, B.M., et al. (2008). Treatment of Late Infantile Neuronal Ceroid

871   Lipofuscinosis by CNS Administration of a Serotype 2 Adeno-Associated Virus Expressing CLN2

872   cDNA. Hum Gene Ther *19*, 463–474.

873

874   Yoshioka, Y., Abe, T., Wakusawa, R., Moriya, T., Mochizuki, S., Saigo, Y., Saito, T., Murata, H.,

875   Tokita, Y., Iseya, T., et al. (2006). Recombinant AAV-Transduced Iris Pigment Epithelial Cell

876   Transplantation May Transfer Vector to Native RPE but Suppress Systemic Dissemination. Invest

877   Ophth Vis Sci *47*, 745–752.

878

879   Yu, W., Mookherjee, S., Chaitankar, V., Hiriyanna, S., Kim, J.-W., Brooks, M., Ataeijannati, Y., Sun,

880   X., Dong, L., Li, T., et al. (2017). Nrl knockdown by AAV-delivered CRISPR/Cas9 prevents retinal

881   degeneration in mice. Nat Commun *8*, 14716.

882

883   Zhang, X., Serb, J.M., and Greenlee, H.M. (2011). Mouse Retinal Development: a Dark Horse Model

884   for Systems Biology Research. Bioinform Biology Insights *5*, 99–113.